Soil Dynamics and Earthquake Engineering xxx (xxxx) xxx–xxx

Contents lists available at ScienceDirect

Soil Dynamics and Earthquake Engineering

journal homepage: www.elsevier.com/locate/soildyn

On the development of novel mitigation techniques against faulting–induced deformation: "Smart" barriers and sacrificial members

Ioannis Anastasopoulos*, Liam Jones

ETH Zürich, Switzerland

ARTICLE INFO

Keywords:
Fault rupture
Earthquake
Mitigation
Soil-structure interaction

ABSTRACT

Contemporary analysis–design methods against faulting can significantly improve life-safety, but the problem of permanent deformation persists. This paper proposes a novel mitigation technique, addressing post-seismic serviceability. A "smart" barrier is employed to divert the fault rupture, introducing a minimum energy path. The "smart" barrier consists of two sheet-pile walls, connected with rows of sacrificial members. The latter are steel rings, whose performance is a function of geometry. The proposed system can be produced in the form of prefabricated panels, and its performance is largely insensitive to site conditions or workmanship. The barrier is compressed, absorbing tectonic deformation with minimum disturbance to the protected structure. The problem is analyzed employing the FE-method, using a thoroughly validated soil constitutive model with strain softening, confirming the efficiency of the mitigation concept. Further analyses demonstrate the use of sacrificial rings to protect continuous bridge decks, being installed between the deck and the bearings.

1. Introduction

Recent major earthquakes, such as Kocaeli and Düzce (Turkey, 1999), Chi-Chi (Taiwan, 1999), Wenchuan (China, 2008), Kaikoura (New Zealand, 2016) and Kumamoto (Japan, 2016) have shown that faulting-induced ground deformation can cause substantial damage to critical infrastructure (e.g., [34,35,33,15,27,20,28]). One such example is shown in Fig. 1, referring to the failure of the Shih Kang dam in Taiwan, due to 9 m of upthrust by the notorious Chelungpu fault during the 1999 Chi-Chi earthquake. However, several examples of satisfactory performance of a variety of structures have also been observed in past earthquakes (e.g., [11,4,5,16]).

Motivated by the need to develop design methods for faulting–hazard mitigation, the interaction of fault ruptures with foundation–structure systems was explored during the QUAKER project. Combining field studies [4,5], centrifuge model tests conducted at the University of Dundee [13], and numerical analyses [8], a thoroughly validated analysis and design methodology has been developed. The foundation system was shown to play a crucial role, with continuous and rigid foundations being advantageous. The concurrent design methods have been applied to a variety of projects, including buildings, bridges, and tunnels (e.g., [1,3,2,9]).

The methods developed so far can significantly improve life-safety, but the problem of permanent deformation (rigid-body rotation) has not been resolved. While the structure may survive, it must subsequently be demolished, imposing severe socio-economic consequences. Particularly for the retrofit of existing structures, the addition of a rigid foundation can be very costly; for monuments it may be practically impossible. Built centuries ago, such structures may be situated in the vicinity of previously unknown faults. Hence, there is a need to devise efficient mitigation schemes, preferably with minimum intervention.

The mitigation strategies that can be found in the literature can be broadly categorized as: (a) foundation strengthening; (b) measures aiming to diffuse fault deformation; and (c) measures aiming to divert the fault rupture path away from the structure [11,17,26,32]. The first strategy simply requires a rigid raft foundation, allowing the structure to rotate as a rigid body without excessive distortion. Such a strategy can be effective for both reverse and normal faults [2,8], but is not practical for retrofit of existing structures. Moreover, rigid body rotation is unavoidable, and hence its post-seismic serviceability is not resolved without significant remedial measures such as foundation re-leveling. The second strategy calls for installation of a ductile fill beneath the foundation, with the aim of diffusing the deformation over a wider area. However, this entails replacement of a substantial soil mass, and can only be applied to new structures.

The third strategy can be seen to offer a major advantage, as it can be readily applied to new and existing structures. Instead of foundation strengthening, a wall barrier can be introduced in order to divert the fault rupture path. Oettle & Bray [26] proposed such a concept of a stiff wall barrier, offering protection against normal faults or a "seismic gap" for reverse faults. Fadaee et al. [17], proposed a further concept: a *weak*

* Corresponding author.
E-mail address: ixa@ethz.ch (I. Anastasopoulos).

https://doi.org/10.1016/j.soildyn.2018.04.052
Received 15 September 2017; Received in revised form 23 April 2018; Accepted 27 April 2018

Fig. 1. Damage to the Shih Kang dam due to 9.1 m of upthrust by the Chelungpu fault during the 1999 Chi-Chi earthquake in Taiwan.

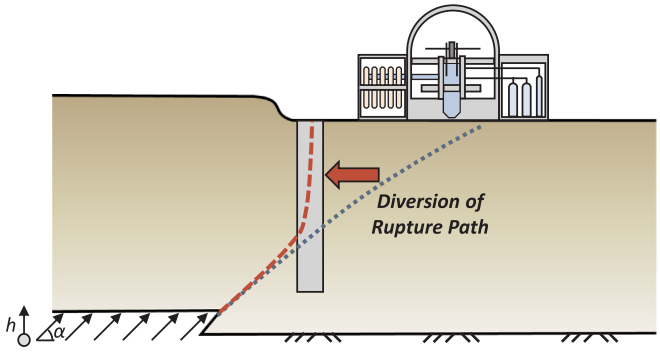

Fig. 2. Concept of weak wall barrier aiming to divert a reverse fault rupture, to protect critical infrastructure.

wall barrier, offering protection against reverse faults (Fig. 2). Since the rupture propagates along a "minimum energy" path [10], such a barrier (weaker and softer than the soil) will act as an "attractor" of plastic deformation and as a "fuse" that absorbs compressive deformation.

This concept has been shown to offer adequate protection in terms of structural integrity, but also substantial reduction of permanent rotation, thus addressing the problem of post-seismic serviceability. In the work of Fadaee et al. [17], the weak wall barrier was materialized by means of a Soil Bentonite Wall (SBW). Such walls are typically used for seepage control under embankment dams or for environmental protection, and can be constructed using diaphragm wall machinery. A shear strength lower than that of the surrounding soil can be achieved using an un-compacted mixture of soil, bentonite, and water as backfill material. Although the SBW was shown, analytically and experimentally, to be very efficient in diverting the fault rupture (Fig. 3), its performance can be sensitive to soil conditions and workmanship. Moreover, its shear strength may increase due to long-term consolidation, thus reducing its capability to act as a barrier.

This paper proceeds one step further, introducing a "smart" barrier: a "fuse" system, consisting of sacrificial members. Such a system can be produced in the form of prefabricated panels, and its (short- and long-term) performance can be reliably predicted. Moreover, consisting of steel members, its properties are largely insensitive to local soil conditions or workmanship. This is an ongoing research and the paper offers a brief overview of the key outcomes of the work conducted so far.

2. Smart barrier with sacrificial members

The concept of the "smart" barrier is similar to the SBW wall, with main difference being the materialization of the "fuse". Instead of using a soil-bentonite-water mixture, a more robust and predictable solution is proposed, consisting of steel sacrificial members sandwiched between sheet pile walls.

In order to explain the main concept, it is useful to draw an analogy to active and passive conditions (Fig. 4). Under static conditions (i.e., before faulting), the wall is subjected to active or at-rest earth pressures, depending on the excavation sequence (Fig. 4**a**). When subjected to reverse faulting-induced deformation, passive earth pressures tend to develop (Fig. 4**b**). As discussed later on, steel rings of diameter D, out-of-plane length L, and thickness t, constitute the simplest form of sacrificial members. The ultimate capacity of such a ring F_{ult} is simply a function of geometry and steel strength. Therefore, each row of rings can be designed to have an adequately large factor of safety against static loading:

$$FS_{st} = F_{ult}/F_0 \geq 1.5 \quad (1)$$

where: F_0 is the lateral force due to in-situ conditions. In a similar manner, each row of rings can be designed for an adequately small "apparent" factor of safety against passive conditions:

$$FS_f = F_{ult}/F_p \leq 1/1.5 \quad (2)$$

where: F_p is the lateral force due to passive conditions. If the rings are designed to yield under such compressive loading, F_p will never develop and this is why FS_f is an "apparent" factor of safety.

Considering the problem as strain-controlled, it becomes evident that the earth pressures that develop along the wall are governed by the imposed lateral deformation. As long as the faulting-induced lateral pressure remains below its passive value, passive conditions will not develop, and the fault rupture will not propagate towards the structure. Instead, the wall is compressed, "absorbing" the faulting-induced deformation by compressive failure of the sacrificial members. Of course, in reality, there is also a vertical component, which translates to shear deformation of the rings. Still though, the main concept remains the same.

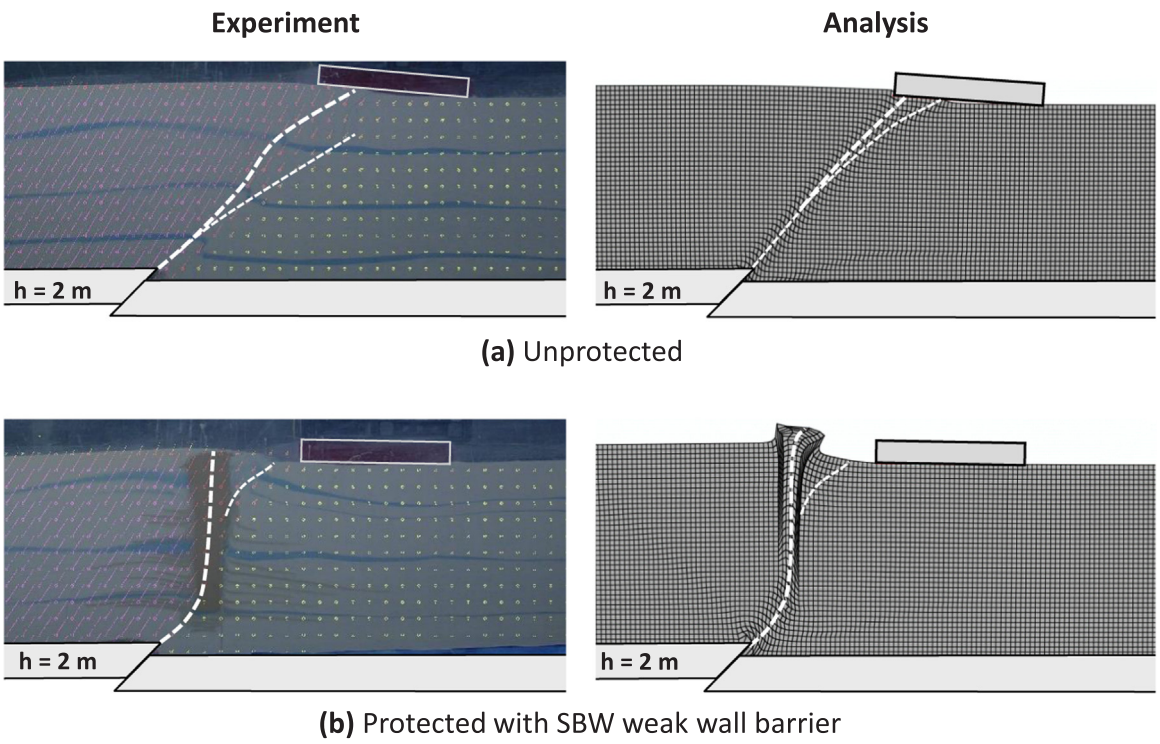

Fig. 3. Example showing the efficiency of fault hazard mitigation with a Soil Bentonite Wall (SBW). Comparison of a $B = 15$ m foundation: (a) unprotected; and (b) protected with a SBW. The deformed physical model (left) is compared to the FE deformed mesh (right) for fault offset $h = 2$ m (adapted from Fadaee et al., 2013).

To achieve such controlled failure, an elastic–perfectly plastic "fuse" is desirable. The "smart" wall barrier needs to fulfill the following criteria:

(a) The wall barrier must be capable of very large volumetric strains, but without any "densification" effects at large strains.
(b) It needs to resist elastically the developing active earth pressures (under static conditions), which vary with depth. Therefore, the capacity F_{ult} of each row of sacrificial members must also vary with depth.
(c) The wall must deform in a perfectly plastic manner, with its F_{ult} remaining constant for very large strains.

Using these criteria, an optimum design can be obtained, combining efficiency with practicality.

These criteria are similar to those required for mitigation of blast loading. One common technique employed in this field is the addition of "sacrificial cladding" to sensitive structures. This sacrificial cladding normally takes the form of prefabricated panels or sheets attached to the external surface of a structure. Such claddings function in a similar

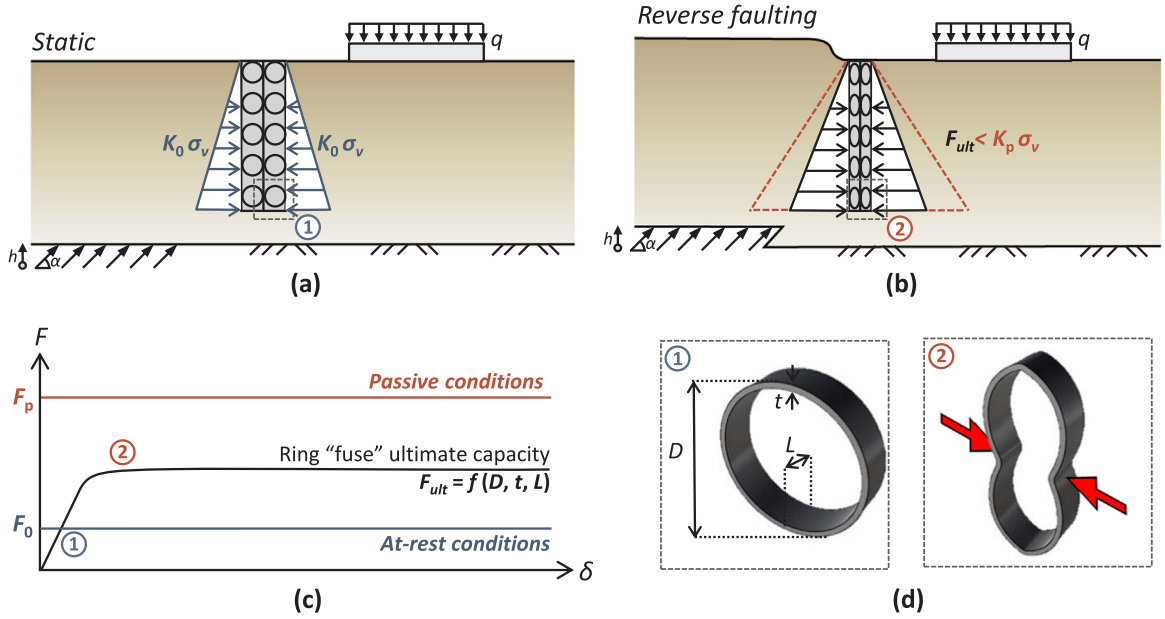

Fig. 4. "Smart" wall barrier concept: (a) before faulting, in-situ (K_0) earth pressures; (b) subjected to reverse faulting, tendency to develop passive (K_p) earth pressures; (c) force-displacement response of a ring-fuse; and (d) main dimensions of a ring fuse and illustration of its compressive failure.

manner to crumple-zones used in modern automotive design; through absorption and dissipation of kinetic energy by means of large plastic deformation. Many such devices are specifically designed to meet certain pre- and post-failure behavioral specifications, including the tailoring of load–displacement behavior. A variety of such designs can be found in the literature [29], along with useful general behavioral performance predictions based on archetypal designs, including, but not limited to, foams, rheological devices and mechanical energy dissipaters. As such, designs and principals from blast loading mitigation are applied to the problem at hand using the previous criteria as a basis for selection.

In order to achieve the first objective (a), the system is treated as a very narrow open excavation, supported by two sheet pile walls, propped at regular depths. Thus, the "densification" effect, as described in sacrificial cladding publications, is minimized. The term "densification" refers to a large decrease in void space in a sacrificial cladding system, due to large global volumetric strain, after which the device behaves more like a rigid plate [18,19,24]; a problem particularly evident in the application of foam claddings, hence the immediate exclusion of geo-foam as a viable solution. By controlling the ultimate capacity F_{ult} of the props (i.e., the sacrificial members), the second objective (b) can be fulfilled. The third objective (c) can be accomplished by considering the ultimate capacity of the "props" at each layer and their post-failure behavior. With this in mind, we refer to the "props" as mechanical sacrificial members, whose primary design is based upon their plastic response.

There are a number of options available in the literature for the design of such sacrificial members. For the sake of simplicity and constructability, the simplest design that replicates the desired perfectly plastic response is proposed. Focusing on protection against blast loading, Calladine and English [14] examined the post failure behavior of two archetypal designs (Types I & II), whose construction (and purpose) is similar to the current study: using very large volumetric deformation and plastic energy dissipation to mitigate large pressures.

Type I and Type II devices (Fig. 5) are defined by their stress–strain (load–deflection) relation. Type II devices act as stiff connectors that undergo significant reduction of strength once plasticity is achieved. Type I devices exhibit perfectly plastic response, reaching a point of plastic capacity and then retaining a constant level of strength with increasing deformation. The previously discussed rings are a typical "Type I" device: an open steel cylinder, loaded along its diameter between two plates. For the problem under study, this design can readily be achieved by installing steel rings between the sheet-pile walls.

The elastic behavior of such steel rings can be calculated as described by Timoshenko & Gere [31]:

$$M_o = \frac{PR}{2}\left(\frac{2}{\pi}-1\right) \tag{3a}$$

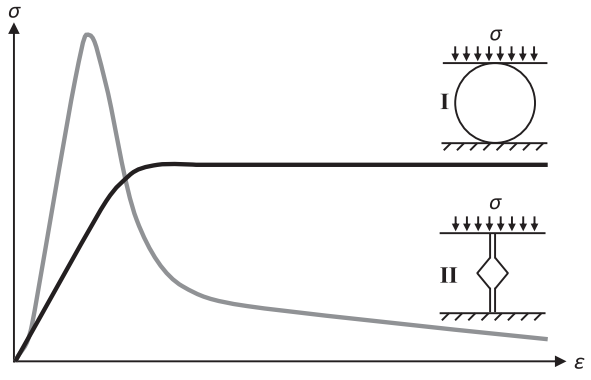

Fig. 5. Proposed stress–strain relations of archetypal sacrifical devices (after [14]).

$$F_{ult} = \frac{1}{2}\bullet\frac{L\bullet t^2\bullet\sigma_y}{R\bullet(\pi/2-1)} \tag{3b}$$

where: M_o is the maximum moment in the cylinder, P is the applied force, and R the ring radius (Eq. 3a). By assuming the wall of the cylinder to behave loosely as a rectangular (F_{ult}) beam section of steel yield strength σ_y, we can see that the ultimate failure capacity of the ring is controlled by varying the wall thickness (t), radius (R) and out of plane length (L) (Eq. 3b). For the sake of simplicity (in terms of constructability), the variation of plastic failure load with depth can be achieved by varying the out of plane length of the ring, keeping all other parameters constant. A suitable out of plane length is selected for every depth, so that the sacrificial member can hold the excavation open (with adequately large FS_{st}), but will yield long before the development of passive earth pressures (with adequately small FS_f).

Such a system can be easily realized employing traditional diaphragm wall construction methods. A trench is excavated in the traditional manner, supported by a bentonite slurry mixture (Fig. 6). Prefabricated sacrificial panels are then lowered or partially driven into the excavation and the bentonite mixture is removed. Thus, what remains is a narrow, deep excavation supported by the sacrificial members. Such a scheme has been discussed with a major contractor, and although it entails certain challenges, it has been deemed constructible using pre-existing diaphragm wall construction techniques and equipment.

3. Numerical simulation

As shown in Fig. 7, the general problem refers to a reverse fault (dip angle α) producing an upthrust of vertical component h, propagating through a soil deposit of thickness H. A raft foundation of width B, with a surcharge load q, is placed at distance s from the unperturbed (i.e., free-field) fault outcrop. A "smart" barrier of height $3H/4$ thickness B_w is positioned at distance L_{SB} from the (left) edge of the foundation.

The problem is analyzed employing the finite element (FE) method. Finite element (FE) modelling has been shown to be capable of efficiently reproducing fault rupture propagation in the free field [12,6], and its interaction with surface and embedded foundations [22,8]. The analysis is conducted employing the FE code ABAQUS. The soil is modelled with quadrilateral continuum elements under plane strain conditions. Following the findings of previous studies, an elastoplastic constitutive model with Mohr-Coulomb failure criterion, non-associated flow rule and isotropic strain softening is adopted [6]. The pre-yield phase of response is linear elastic, with a secant modulus $G_s = \tau_y/\gamma_y$ increasing linearly with depth. Strain softening is introduced by reducing the mobilized friction angle φ_{mob} and the mobilized dilation angle ψ_{mob} with the increase of octahedral plastic shear strain (Fig. 8) using a non-associated flow rule and the following relationships:

$$\varphi_{mob} = \begin{Bmatrix} \varphi_P - \frac{\varphi_P-\varphi_{res}}{\gamma_f^P} & for\ \ 0\le\gamma_{oct}^P < \gamma_f^P \\ \varphi_{res} & for\ \ \gamma_{oct}^P \ge \gamma_f^P \end{Bmatrix} \tag{4}$$

$$\psi_{mob} = \begin{Bmatrix} \psi_P\left(1-\frac{\gamma_{oct}^P}{\gamma_f^P}\right) & for\ \ 0\le\gamma_{oct}^P < \gamma_f^P \\ \psi_{res} & for\ \ \gamma_{oct}^P \ge \gamma_f^P \end{Bmatrix} \tag{5}$$

where: φ_P, φ_{res} and ψ_P, ψ_{res} are the maximum (p) and ultimate residual (res) (critical state) friction and dilation angles respectively; and γ_{oct}^P, γ_f^P are the octahedral shear strains (in which f denotes the strain at which softening is completed). The constitutive model is calibrated using shear box tests and has been thoroughly validated through Class "A" blind predictions of centrifuge test conducted at the University of Dundee [6,8].

The foundation raft is simulated with linear elastic beam elements. A tensionless contact interface is used to realistically simulate detachment and sliding of the foundation relative to the soil (Fig. 8). The

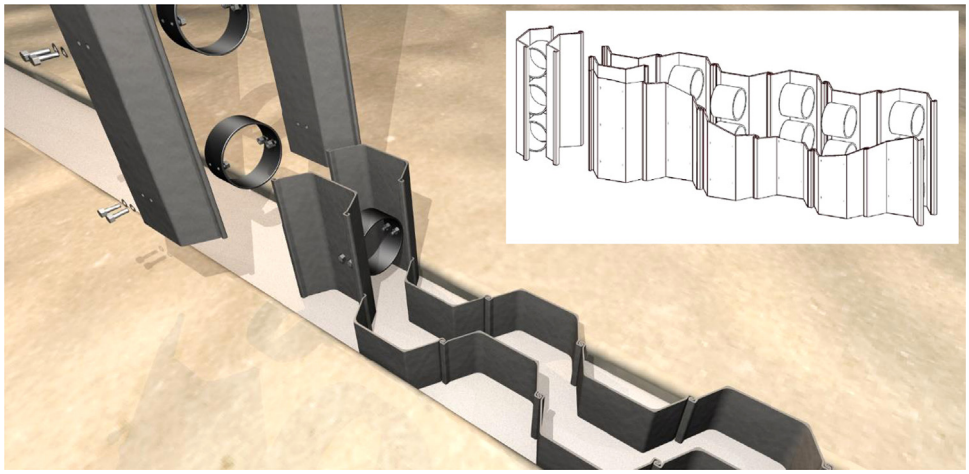

Fig. 6. Conceived construction process: the panels are assembled from conventional sheet-pile walls and circular hollow sections (sacrificial fuses) before being lowered into the bentonite supported excavation pit.

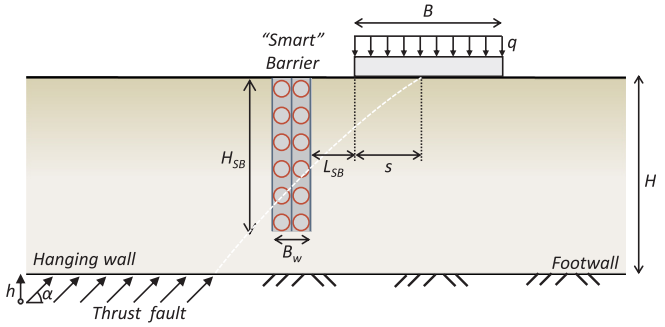

Fig. 7. Problem definition and key parameters: interaction of a thrust fault rupture, propagating through an $H = 20$ m soil deposit, with a slab foundation of width B, carrying a surcharge load q, positioned at distance s from the theoretical point of rupture outcropping in the free field protected with a "Smart Barrier" (SB) of thickness B_w and depth H_{SB}.

"smart" barrier is also modelled with beam elements, which are however nonlinear in order to model the limited ultimate capacity of the Type I sacrificial rings. The sheet pile walls are simulated with beam elements, rigidly connected to the soil elements along the depth of the excavation (Fig. 9). Given the compressive nature of the thrust faulting deformation, sliding at the sheet pile–soil interface is considered improbable, and it was therefore tactically ignored. The sacrificial rings are discretized in 24 nonlinear beam elements (Fig. 9). An elastic-perfectly plastic constitutive law is employed, which was shown to be sufficient to produce the desired perfectly plastic global response. The capacity of the sacrificial rings varies with depth, by simply specifying regular increments of out of plane length (here: beam width) for each depth, aiming to achieve the desired safety factors FS_{st} and FS_f.

A detailed parametric study was conducted and its detailed results can be found in Jones [21]. Different scenarios and barrier configurations were investigated, varying the free field outcrop location (s), sacrificial member ultimate capacity (FS_f) and barrier breadth (B) with a fault dip angle $\alpha = 60^0$. In each case faulting is applied in steps of h/H = 1% from 0% to 5%. An example is shown in Fig. 7, referring to a rigid $B = 10$ m foundation with $q = 20$ kPa subjected to $h = 1$ m thrust faulting at $s = 5$ m propagating through an idealized dense sand layer of $H = 20$ m thickness.

The comparison is performed in terms of deformed mesh with superimposed plastic strain contours along with the computed foundation rotation (Fig. 10**a**). The unprotected reference case is compared to protection with a SBW and to the proposed "smart" barrier with sacrificial rings. Both the "smart" barrier and the SBW effectively divert the fault rupture away from the foundation. The sacrificial devices perform as expected; sustaining plastic failure soon after the faulting deformation begins (in the specific case, plastic capacity is reached at $h/H \approx 2\%$). The differences in terms of rotations are quite substantial. The unprotected foundation sustains rotation $\theta \approx 3^\circ$, a value that is clearly beyond reasonable serviceability limits. The SBW-protected foundation performs appreciably better, with its rotation θ not exceeding 0.4°. The performance of the "smart" barrier is even better, with $\theta \approx 0.2^\circ$.

As shown in Fig. 10**b**, the same conclusions can be drawn based on the normalized contact pressures p/q and foundation bending moments . Faulting induces hogging and sagging moments through loss of support in the unprotected case, and at high offsets for the SBW. Without any mitigation measures, this induced bending moment is almost 5 times larger than the static value, something that would imply failure in reality. The SBW reduces substantially the distress of the foundation, but still is about 2 times larger than the initial static value. The "smart"

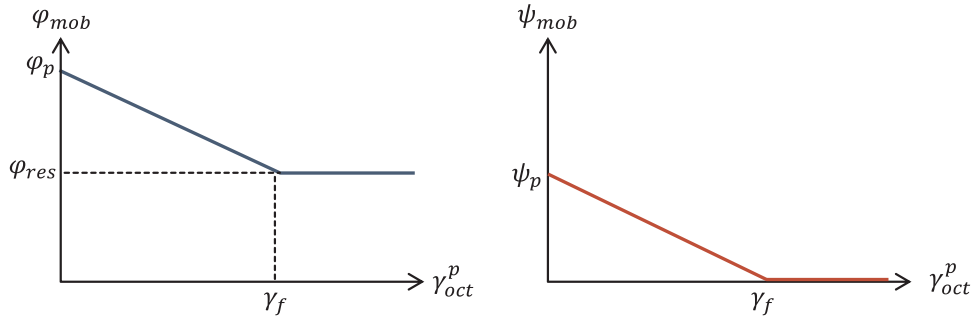

Fig. 8. Mohr-Coulomb model with strain softening: variation of mobilized friction (φ) and dilation angle (ψ) with octahedral plastic shear strain (γ^p_{oct}).

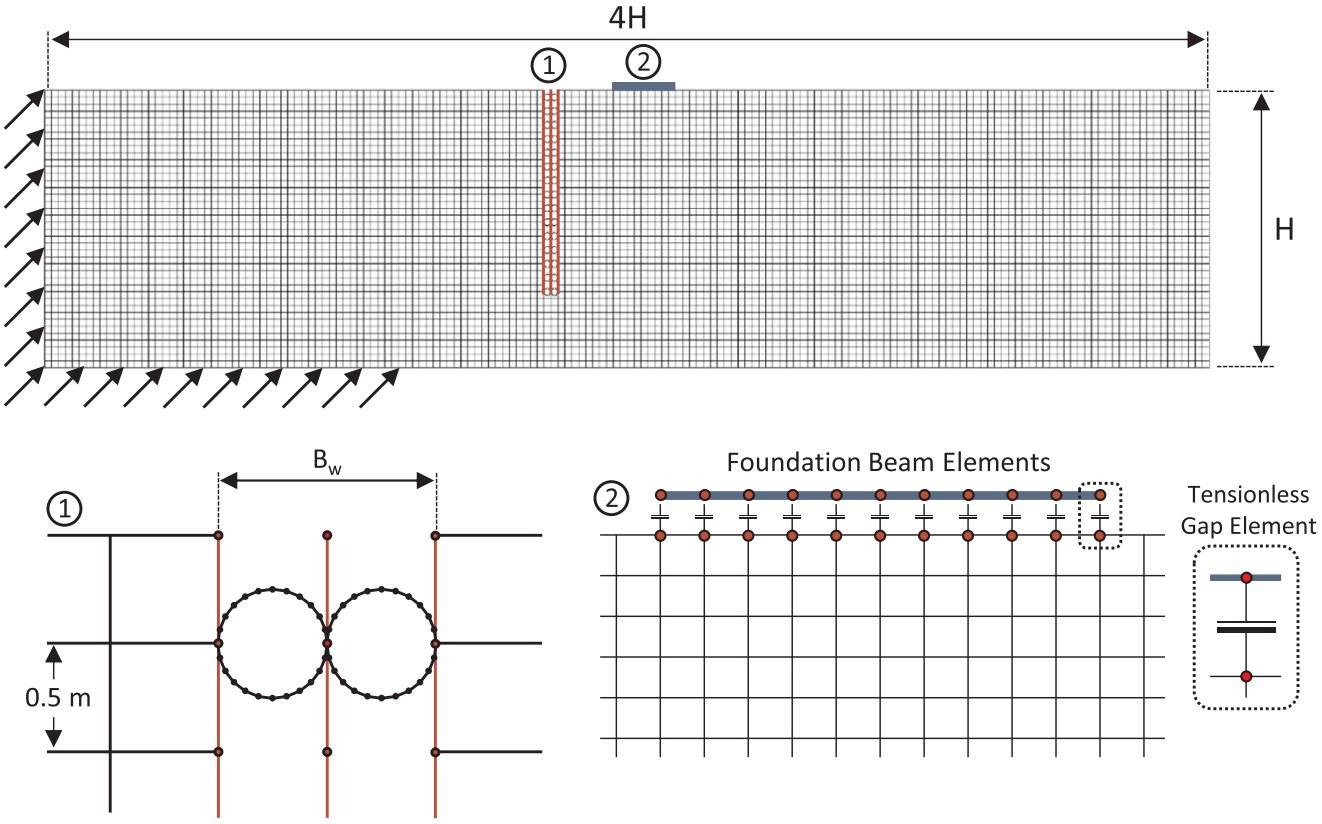

Fig. 9. Finite element model: an aspect ratio of 4:1 is employed to minimise parasitic boundary effects. Sheet pile walls and sacrificial members are modelled with elastic-perfectly plastic beam elements; elastic beam elements are employed for the foundation, which is connected to the soil with tensionless gap elements.

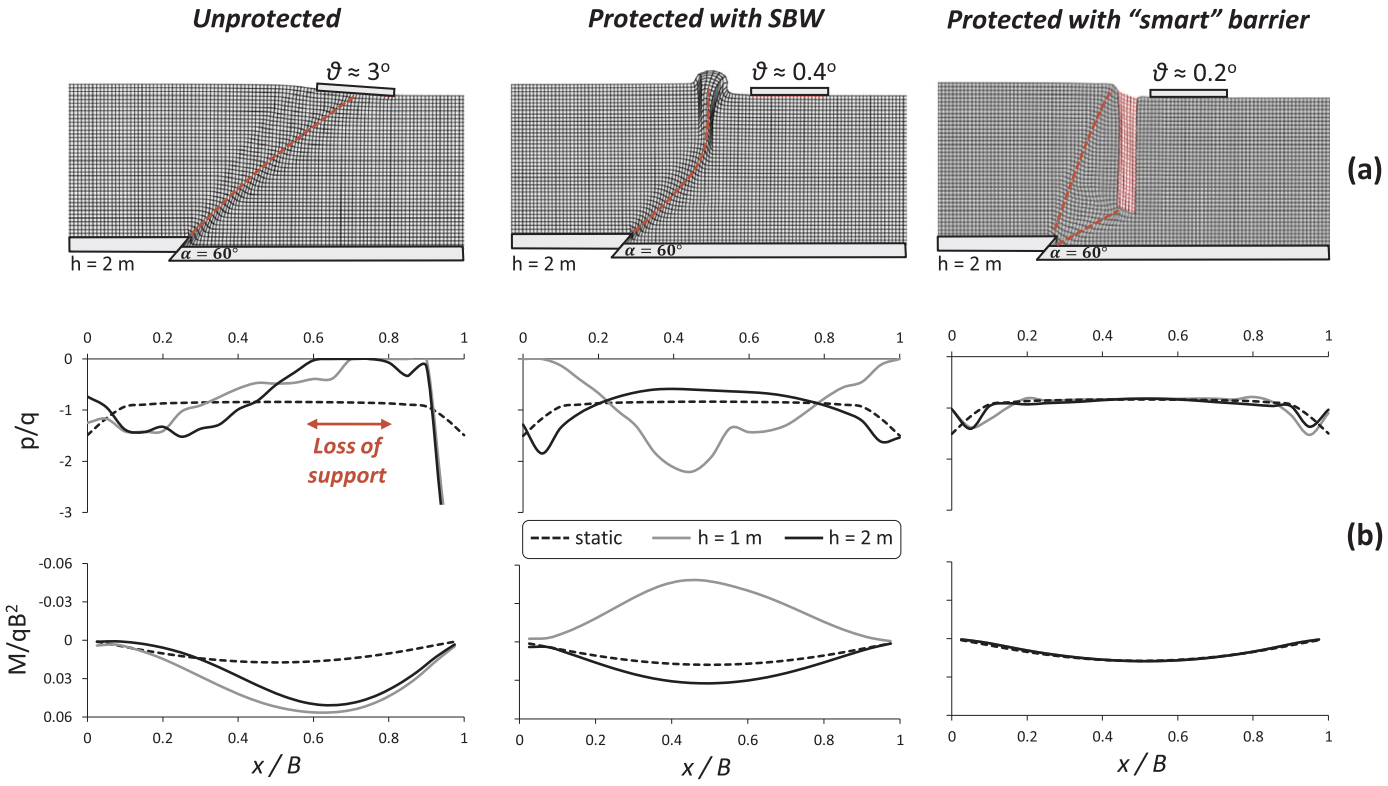

Fig. 10. Efficiency of faulting hazard mitigation using a $B_w = 3$ m *"smart" barrier* for a $B = 10$ m foundation carrying $q = 20$ kPa surcharge load, positioned at distance $s = 5$ m. Comparison of the unprotected case (left) with a *Soil Bentonite Wall – SBW* (middle), and the proposed "smart" barrier: (a) deformed mesh ($h = 2$ m); and (b) normalized contact pressures p/q foundation bending moment M/qB^2 along the width of the foundation.

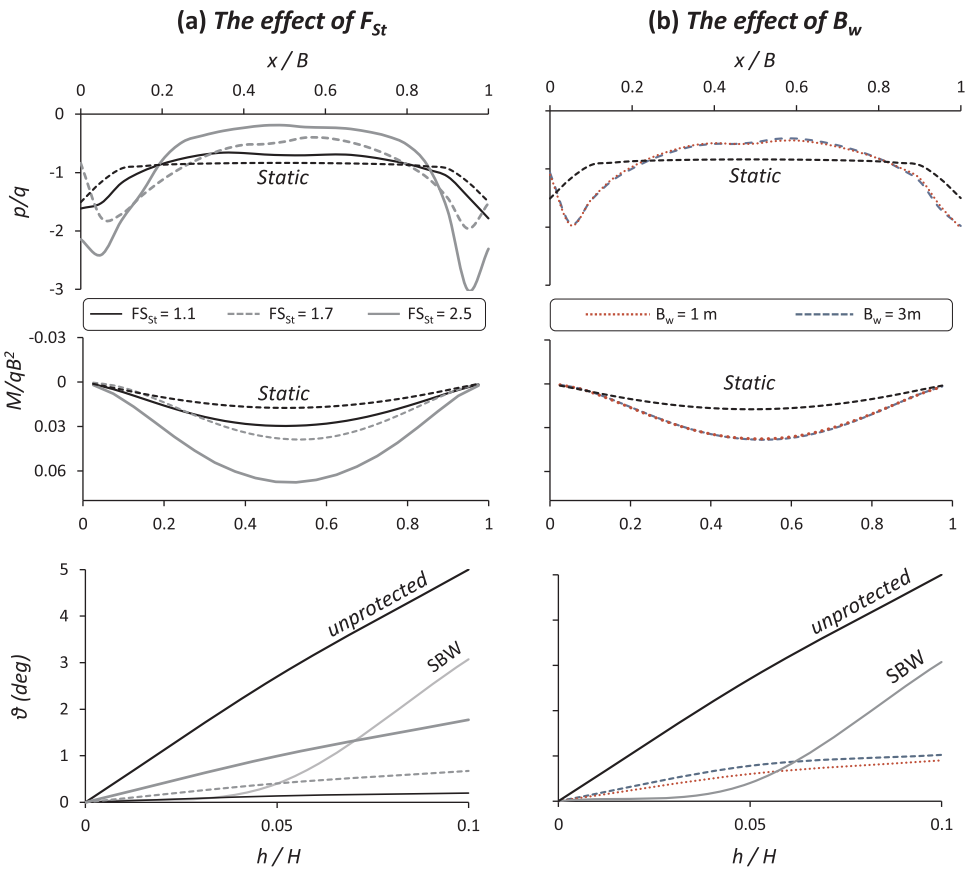

Fig. 11. (a) The effect of the factor of safety of the rings against static loading FS_{St}; and (b) the effect of the breadth B_w of the "smart" barrier system for a $B = 10$ m foundation carrying $q = 20$ kPa surcharge load, positioned at $s = 9$ m, for a fault offset of h $= 2$ m. Normalized contact pressures p/q along the foundation (top); normalized foundation bending moment M/qB^2 (middle); and evolution of rotation θ with normalized bedrock fault offset h/H (bottom).

barrier is clearly the most efficient, with the bending moment being practically insensitive to the imposed dislocation. Normalized contact pressures (Fig. 10**b**) show how the foundation remains in contact with the soil as if no fault had occurred.

Further investigation was made on both the effect of the ultimate capacity of the sacrificial rings, expressed through the factor of safety against static loading FS_{st} and the width of the "smart" barrier system B_w. Fig. 11 shows indicative results from one analyzed case, for a $B = 10$ m foundation carrying a surcharge load $q = 20$ kPa, positioned at $s = 9$ m. This case was selected due to the particularly large distress of the foundation that was observed in the unprotected case. Fig. 11**a** depicts the effect of increasing the ultimate capacity F_{ult} of the sacrificial members, plotted in function of FS_{st} (Eq. (1)). Variations in ultimate capacity can be seen to have a predictable impact on performance: the stronger the sacrificial rings, the more faulting deformation is allowed to propagate to the structure before plastic failure in the smart barrier is reached and the device is "activated", mitigating further damage to the structure.

Interestingly, as the failure capacity approaches the passive resistance of the soil–foundation system ($FS_{st} \geq 2.5$), the faulting–induced stressing and the rotation of the foundation seem to reduce when compared to weaker systems. Upon investigation, this is seen to be a result of the sacrificial system acting as a rigid "wall" when the sacrificial elements do not fail. In such a case, the fault rupture propagates to the ground surface by pushing the entire barrier upwards and to the right, which tends to move more-or-less as a rigid body in a way similar to passive failure of a conventional retaining wall. Given that the foundation lies on-top of the developing passive wedge, the entire soil–foundation system can be seen to displace up and to the right, effectively as a rigid block, not sustaining any substantial distress or rotation. However, this is the case only for a relatively narrow foundation, such as the one investigated herein. Should the structure be any wider, such that part of it lies outside the developing passive wedge, the (practically rigid) barrier would not offer any appreciable protection.

As shown in Fig. 11**b**, the performance appears to be insensitive to the width B_w of the "smart barrier". The figure compares the normalized contact pressures p/q and foundation bending moments , as well as the evolution of foundation rotation θ with normalized bedrock fault offset h/H for the same configuration as previously, varying B_w from 1 m to 3 m. There are some small discrepancies, which are observable only for relatively small fault offsets. These are due to differences in the elastic deformation of the sacrificial wall system, which lead to some minor differences in foundation performance. The larger breadth wall (B_w= 3 m) undergoes increased elastic deformation before activation (i.e., failure) of the sacrificial members, leading to slightly higher induced stressing of the foundation.

Some of the observed discrepancies between different widths are due to the fact that the distance between the foundation and the barrier is kept constant. Thus, as the wall thickness B_w is increased, the left edge of the "smart" barrier moves closer to the bedrock dislocation for a given position s. Overall, the increase of B_w leads to minor improvement of performance. However, this conclusions is only valid when B_w is larger than the horizontal component of the imposed fault offset, as in the cases examined herein. The maximum deformation that can be absorbed by the "smart" barrier cannot be larger than its breadth B_w.

Another interesting point to note is the specific fault rupture mechanism (Fig. 10**a**). Where both the unprotected and SBW cases propagate at a similar trajectory, the "smart" barrier case can be seen to be markedly different. Here, the fault is not propagating at its free–field trajectory, but appears to bifurcate immediately. This is due to the transfer from a pure shear event (as in the unprotected and SBW cases) to a more mechanistic phenomenon. Specifically, the fault will not propagate to the mid height of the wall, because upon "hitting" the wall the fault would then have to shear the whole barrier system, including the very stiff sheet pile walls. This requires significantly more energy than producing the kind of sliding-wedge mechanism observed in the

analysis. Thus, the barrier does not simply provide a new "path of least resistance" as in the SBW case, but creates a new, fundamentally different, lower energy failure mechanism, formed of sliding blocks of soil. The "smart" barrier forces the soil layer to behave as two rigid blocks, one moving and one stationary, with a perfectly plastic spring connecting them.

In all cases examined here, the smart barrier outperforms the soil bentonite wall system, especially for larger fault offsets ($h/H > 5\%$). The improvement over the unprotected case is significant, both in terms of foundation distress (expressed through the normalized bending moment ,) and permanent rotation θ. In combination with the apparent insensitivity to wall thickness (for the examined $h = 1$ m maximum fault offset; for larger fault offsets, an increase of the wall width would definitely be necessary), this implies that the proposed smart barrier may offer a simple and economically efficient faulting hazard mitigation solution.

Although providing large improvements in large fault offset scenarios, the described system may well not be appropriate for smaller events, where the cost and complexity of the system may outweigh the benefit to any protected structure. Thus, it is worth examining when such a system should be employed. Most superficially, it can be seen that the "smart" barrier is not significantly advantageous over other methods (or even the unprotected case in terms of induced forces in the foundation) for very small fault offsets (here $h/H < 3\%$). Thus, this offset could be proposed as a "threshold" value, possible exceedance of which would warrant the installation of the device. However, predicting the offset of a fault a priori is not an easy task, especially when, as here, the required accuracy is of the order of 0.1 m (from $h/H =$ 2–3% presented here is 0.2 m). This is further complicated by the fact that the "activation", or the point at which the sacrificial members fail and the system becomes effective, is a direct function of the specified static factor of safety (FS_s). Thus, the system could be designed to be activated at very small fault offsets, provided that the static factor of safety is acceptable. Instead, it is likely that installation of such a system would be specified by the importance of the protected structure, and precisely how critical post-seismic serviceability is. Such a case may be a nuclear power station, where there is zero tolerance of structural disturbance, and any improvement in performance during fault events is highly desirable, regardless of the magnitude of the event.

A small number of indicative cases have been presented here, illustrating the interesting and unique behavior of such a system. Although presented at the opening stages of conceptualization, further detailed analysis of the system and its effectiveness is planned.

4. Sacrificial members for bridges

The same concept can be applied for the protection of a bridge deck, as schematically illustrated in Fig. 12. The selected example refers to an existing motorway overpass bridge with a continuous multi-span deck (Fig. 12**a**). More specifically, the bridge is a five span system with a total length of 115.6 m. Increased complexity is added due to the asymmetry of the structure, due to the varying length of the spans (from 18.9 m to 30 m), the different pier heights, and the pier-deck connections. In the initial design (without sacrificial devices), the prestressed concrete deck is monolithically connected to piers P3 and P4, resting on sliding bearings at piers P1 and P2, and on four elastomeric bearings at each abutment.

As discussed in Anastasopoulos et al. [7], such an indeterminate static system is sensitive to tectonic deformation, and simply-supported decks would be the simplest logical solution. However, this is not efficient in terms of static loading, and requires a large number of joints, designed for large deformations. Sacrificial rings can be installed between the top of the piers and the bearings. These members are once again designed to elastically resist the static loads (dead weight and traffic loads) during normal serviceability conditions, and to yield shortly after faulting-induced deformation begins.

The bridge-foundation-soil system is modelled in 3D (Fig. 12**b**), employing the same strain softening constitutive model. The seismic performance of the bridge is analyzed employing the FE method. The deck and the piers are modelled with elastic and inelastic beam elements, respectively. The inelastic behavior of the piers is simulated with a nonlinear model, calibrated against the results of RC section analysis using the USC-RC software. Linear elastic springs are used to model the compression and shear stiffness of the bearings. The footings and the abutments are modelled with elastic hexahedral continuum elements, assuming the properties of reinforced concrete ($E = 30$ GPa).

A detailed parametric study was conducted for a number of cases and the detailed results can be found in Lupis [23]. An example comparison is shown in Fig. 13**a**, referring to a thrust fault of vertical offset $h = 1$ m with a dip of $\alpha = 60^0$ outcropping between piers P1 and P2.

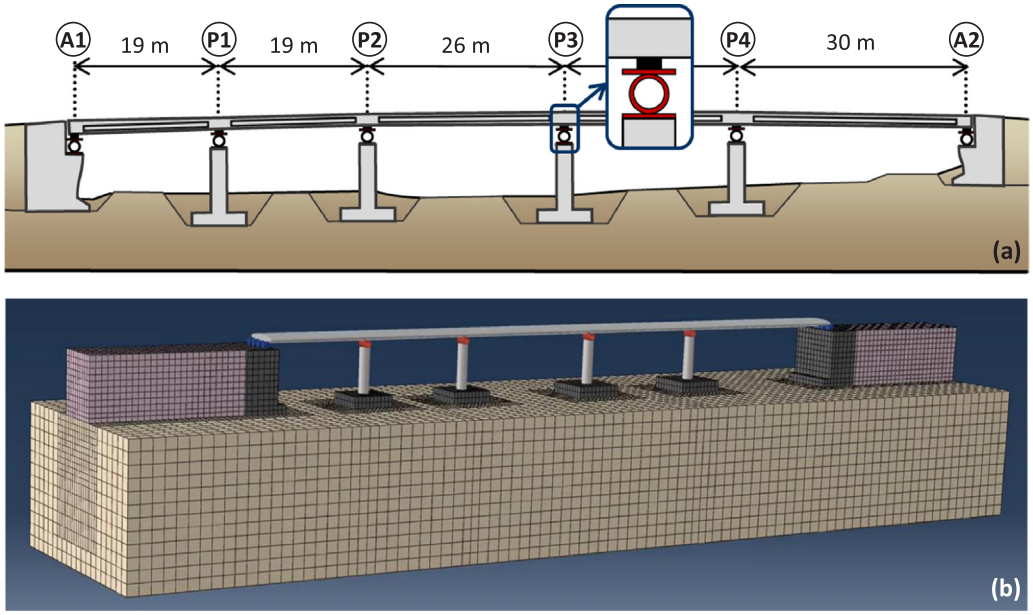

Fig. 12. Application of sacrificial members to a motorway bridge: (a) longitudinal cross-section, along with the conceived installation of the sacrifical members; and (b) 3D FE model of the bridge–abutment–foundation soil system.

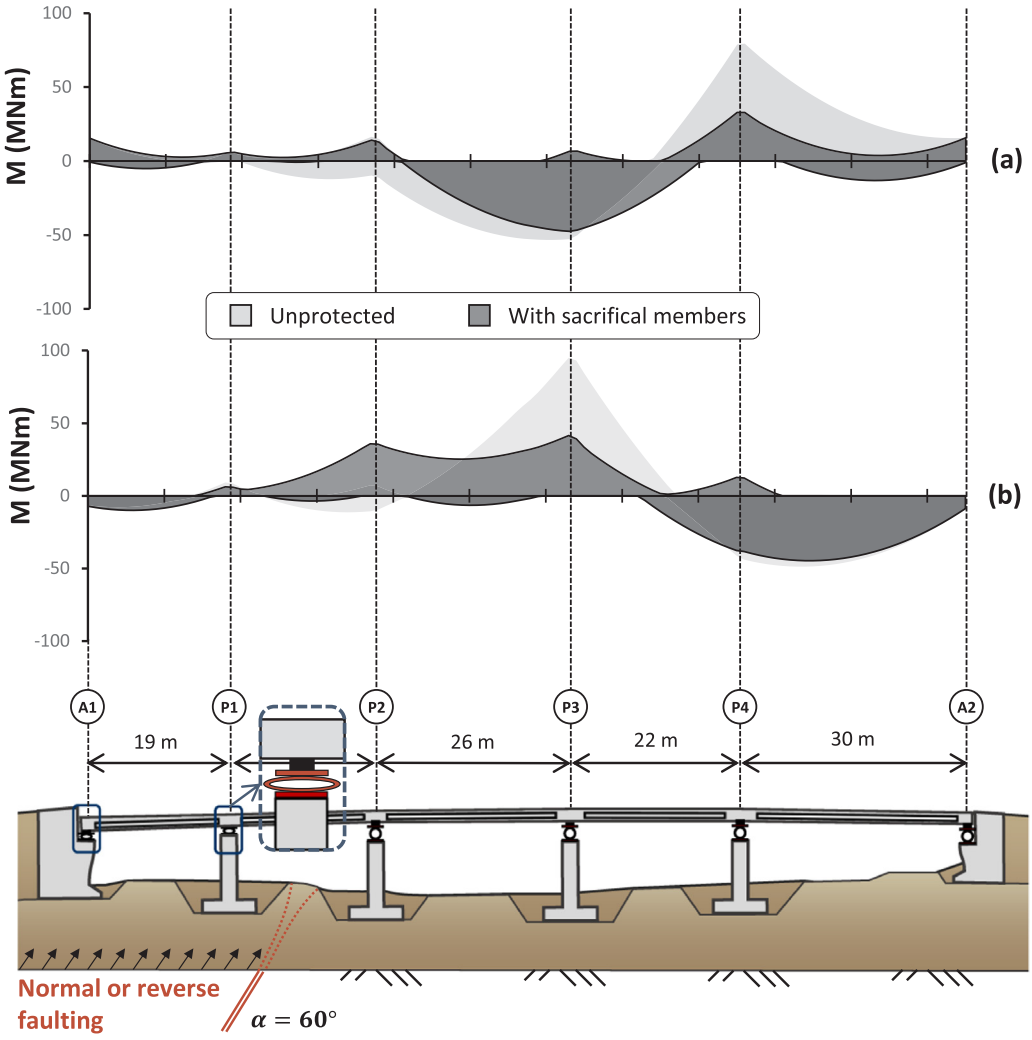

Fig. 13. Efficiency of sacrificial members in protecting a continuous bridge deck subjected to $h = 1$ m faulting. Comparison of deck bending moments with and without sacrificial members for: (a) normal faulting between piers P1 and P2; and (b) reverse faulting between piers P1 and P2. Illustration is indicative of reverse faulting behavior.

The aim of the mitigation is to limit the bending moment of the continuous deck, by allowing for controlled plastic deformation of the sacrificial members. Due to the differential displacement of the piers, the vertical forces which are transmitted to the sacrificial members tend to change: some of the piers may be subjected to unloading and some to increased loading. In the latter case, the corresponding sacrificial rings will be activated (i.e., fail) protecting the deck from excessive flexural distortion. The peak deck bending moments are substantially reduced with the addition of the sacrificial rings, from about 80 MNm in the unprotected case, to just over 30 MNm with the sacrificial members. This is considered a pronounced difference, showing that the concept of sacrificial members can be employed to protect continuous deck bridges. The efficiency of the conceived mitigation technique is similar for the case of a normal fault having the same offset and dip as previously, as shown in Fig. 13**b**.

5. Conclusions

The paper has outlined a novel seismic hazard mitigation technique, with the goal of protecting critical infrastructure against faulting-induced deformation. In the case of buildings, this is achieved by installing a "smart" barrier between the structure and the outcropping fault rupture, aiming to divert the rupture path. Since the fault rupture follows a path of minimum energy, such a weak wall barrier will act as an attractor of plastic deformation.

The "smart" barrier is a "fuse" system, consisting of two thin sheet-pile walls (parallel to each other) with multiple rows of sacrificial members acting as elastoplastic struts. The latter are simple steel rings, the ultimate capacity F_{ult} of which can be reliably determined by adjusting their diameter D, out of plane thickness L, or wall thickness t. Such a system can easily be produced in the form of prefabricated panels, and its (short- and long-term) performance can be reliably predicted. Consisting of steel members only, its properties do not rely so heavily on local soil conditions and workmanship as a bentonite system. The presence of water may raise issues with regard to corrosion, but it should not be expected to alter the performance of the barrier.

Each row of rings is designed to have an adequately large factor of safety against static loading, and an adequately small "apparent" factor of safety against passive conditions. In this way, the rings can safely sustain the static loads, but will yield in a controllable manner when subjected to compressive loading, due to thrust faulting. In such a case, the "smart" barrier is compressed, absorbing the faulting-induced deformation. In addition, the "smart" barrier needs to be designed to resist soil pressures and deformations due to seismic shaking, an issue which has not been addressed herein. The behavior of such systems under dynamic loading is a complex phenomenon, but based on the available literature (e.g., [30,25]) it would appear that accounting for this would require modification to the specification of the "static" factor of safety

through a change in the distribution of active earth pressures, although this change may not be as significant as once thought for such as system as depicted here.

The problem was analyzed employing the FE method, using a thoroughly validated soil constitutive model with strain softening. The results confirm the efficiency of the proposed mitigation concept, both in terms of structural integrity, and with respect to the reduction of permanent foundation rotation. Therefore, the proposed “smart” barrier mitigation technique also addresses the problem of post-seismic serviceability. Although presented here as a two-dimensional case, initial extensions into 3D have also highlighted interesting phenomena, such as the required width of such a system relative to its protected structure (roughly twice as wide). This 3D behavior further highlights the numerous potential avenues of exploration remaining for such a concept in addition to those presented here.

The same principle can be employed to protect bridges with a continuous deck. The sacrificial devices can be installed between the deck and the bearings, designed according to the same principles. The efficiency of the mitigation technique has been explored by 3D FE analysis of an existing motorway bridge. It was shown that the installation of sacrificial rings leads to a pronounced reduction of deck bending moments.

References

[1] Anastasopoulos I, Gazetas G. "Design Against Fault Rupture: Methodology and Applications in Greece", *Proceedings of the 1st Greece – Japan Workshop: Seismic Design, Observation and Retrofit of Foundations*, Athens, Octobe 2005 11-12; 2005. p. 345–366.

[2] Anastasopoulos I, Antonakos G, Gazetas G. Slab foundation subjected to thrust faulting in dry sand: parametric analysis and simplified design method. Soil Dyn Earthq Eng 2010;30(10):912–24.

[3] Anastasopoulos I, Callerio A, Bransby MF, Davies MCR, El Nahas A, Faccioli E, Gazetas G, Masella A, Paolucci R, Pecker A, Rossignol E. Numerical analyses of fault–foundation interaction. Bull Earthq Eng 2008;6(4):645–75.

[4] Anastasopoulos I, Gazetas G. Foundation-structure systems over a rupturing normal fault: part I. Observations after the Kocaeli 1999 Earthquake. Bull Earthq Eng 2007;5(3):253–75.

[5] Anastasopoulos I, Gazetas G. Foundation–structure systems over a rupturing normal fault: part II. Analysis of the Kocaeli case histories. Bull Earthq Eng 2007;5(3):277–301.

[6] Anastasopoulos I, Gazetas G, Bransby MF, Davies MCR, El Nahas A. Fault rupture propagation through sand: finite-element analysis and validation through centrifuge experiments. J Geotech Geoenviron Eng 2007;133(8):943–58.

[7] Anastasopoulos I, Gazetas G, Drosos V, Georgarakos T, Kourkoulis R. Design of bridges against large tectonic deformation. Earthq Eng Eng Vib 2008;7(4):345–68.

[8] Anastasopoulos I, Gazetas G, Bransby MF, Davies MCR, El Nahas A. Normal fault rupture interaction with strip foundations. J Geotech Geoenviron Eng ASCE 2009;135(3):359–70.

[9] Anastasopoulos I, Gazetas G. Analysis of cut-and-cover tunnels against large tectonic deformation. Bull Earthq Eng 2010;8(2):283–307.

[10] Berrill J. Two-dimensional analysis of the effect of fault rupture on buildings with shallow foundations. Int J Soil Dyn Earthq Eng 1983;2(3):156–60.

[11] Bray JD. "Developing mitigation measures for the hazards associated with earthquake surface fault rupture". *Workshop on seismic fault-induced failures—possible remedies for damage to urban facilities*. University of Tokyo Press; 2001.

[12] Bray JD, Seed RB, Seed HB. Analysis of earthquake fault rupture propagation through cohesive soil. J Geotech Eng 1994;120(3):562–80.

[13] Bransby MF, Davies MCR, El Nahas A, Nagaoka S. Centrifuge modelling of normal fault–foundation interaction. Bull Earthq Eng 2008;6(4):585–605.

[14] Calladine CR, English RW. Strain-rate and inertia effects in the collapse of two types of energy-absorbing structure. Int J Mech Sci 1984;26(11):689–701.

[15] Erdik M. Report on 1999 Kocaeli and Duzce (Turkey) earthquakes. Struct Control Civ Infrastruct Eng: World Sci 2001:149–86.

[16] Faccioli E, Anastasopoulos I, Gazetas G, Callerio A, Paolucci R. Fault rupture–foundation interaction: selected case histories. Bull Earthq Eng 2008;6(4):557–83.

[17] Fadaee M, Anastasopoulos I, Gazetas G, Jafari MK, Kamalian M. Soil bentonite wall protects foundation from thrust faulting: analyses and experiment. Earthq Eng Eng Vib 2013;12(3):473–86.

[18] Guruprasad S, Mukherjee A. Layered sacrificial claddings under blast loading Part I—analytical studies. Int J Impact Eng 2000;24(9):957–73.

[19] Guruprasad S, Mukherjee A. Layered sacrificial claddings under blast loading part II—experimental studies. Int J Impact Eng 2000;24(9):975–84.

[20] Kiyota T, Ikeda T, Konagai K, Shiga M. Geotechnical damage caused by the 2016 Kumamoto earthquake, Japan. ISSMGE Int J Geoengin Case Hist 2017;4(2):78–95.

[21] Jones L. Seismic “smart” barriers for retrofit of key structures against fault induced failure [Honours thesis]. UK: University of Dundee; 2015.

[22] Loli M, Anastasopoulos I, Bransby MF, Waqas A, Gazetas G. Caisson foundations subjected to reverse fault rupture: centrifuge testing and numerical analysis. J. Geotech Geoenviron Eng ASCE 2011;137:914–25.

[23] Lupis V. Interaction of fault rupture with foundation–structure systems [M.Sc. Dissertation]. University of Genova; 2015. [ERASMUS, Univ. of Dundee].

[24] Ma GW, Ye ZQ. Analysis of foam claddings for blast alleviation. Int Conf Impact Load Lightweight Struct 2007;34(1):60–70.

[25] Mikola RG, Sitar N. Seismic earth pressures on retaining structures in cohesionless soils. Calif Dep Transp 2013.

[26] Oettle NK, Bray JD. Geotechnical mitigation strategies for earthquake surface fault rupture. J Geotech Geoenviron Eng 2013;139(11):1864–74.

[27] Pamuk A, Kalkan E, Ling H. Structural and geotechnical impacts of surface rupture on highway structures during recent earthquakes in Turkey. Soil Dyn Earthq Eng 2005;25(7):581–9.

[28] Shirahama Y, Yoshimi M, Awata Y, Maruyama T, Azuma T, Miyashita Y, Otsubo M. Characteristics of the surface ruptures associated with the 2016 Kumamoto earthquake sequence, central Kyushu, Japan. Earth Planets Space 2016;68(1):191.

[29] Shukla A. Blast mitigation: experimental and numerical studies 2014. New York: Springer; 2014.

[30] Sitar N, Mikola RG, Candia G. Seismically induced lateral earth pressures on retaining structures and basement walls. Geotech Eng State Art Pract: Keynote Lect GeoCongress 2012;2012:335–58.

[31] Timoshenko SP, Gere JM. Theory of elastic stability. Courier Corporation; 2012.

[32] Tolga Yilmaz M, Paolucci R. Earthquake fault rupture—shallow foundation interaction in undrained soils: a simplified analytical approach. Earthq Eng Struct Dyn 2007;36(1):101–18.

[33] Ulusay R, Aydan O, Hamada M. The behaviour of structures built on active fault zones: examples from the recent earthquakes of Turkey. Struct Eng Earthq Eng 2002;19(2):149–67.

[34] Ural D. "The 1999 Kocaeli and Duzce earthquakes: lessons learned and possible remedies to minimize future Losses. Proceedings, Workshop on seismic Fault induced failures, Tokyo, Japan; 2001.

[35] Youd T, Bardet J-P, Bray JD. Kocaeli, Turkey, earthquake of August 17, 1999 reconnaissance report. Earthq Spectra 2000;16.